frontiers | Frontiers in Molecular Neuroscience

TYPE Original Research
PUBLISHED 01 March 2024
DOI 10.3389/fnmol.2024.1222935

OPEN ACCESS

EDITED BY
Tomoyuki Yoshida,
University of Toyama, Japan

REVIEWED BY
Kazuhiro Sohya,
Saga University, Japan
Davide Comoletti,
Victoria University of Wellington,
New Zealand

*CORRESPONDENCE
Henry Houlden
✉ h.houlden@ucl.ac.uk
Jun Aruga
✉ aruga@nagasaki-u.ac.jp
Wei Lu
✉ luw4@mail.nih.gov

RECEIVED 15 May 2023
ACCEPTED 02 February 2024
PUBLISHED 01 March 2024

CITATION
Efthymiou S, Han W, Ilyas M, Li J, Yu Y, Scala M, Malintan NT, Ilyas M, Vavouraki N, Mankad K, Maroofian R, Rocca C, Salpietro V, Lakhani S, Mallack EJ, Palculict TB, Li H, Zhang G, Zafar F, Rana N, Takashima N, Matsunaga H, Manzoni C, Striano P, Lythgoe MF, Aruga J, Lu W and Houlden H (2024) Human mutations in *SLITRK3* implicated in GABAergic synapse development in mice. *Front. Mol. Neurosci.* 17:1222935. doi: 10.3389/fnmol.2024.1222935

Human mutations in *SLITRK3* implicated in GABAergic synapse development in mice

Stephanie Efthymiou[1,2], Wenyan Han[3], Muhammad Ilyas[4], Jun Li[3], Yichao Yu[5], Marcello Scala[1,6,7], Nancy T. Malintan[1], Muhammad Ilyas[8], Nikoleta Vavouraki[9,10], Kshitij Mankad[11,12], Reza Maroofian[1], Clarissa Rocca[1], Vincenzo Salpietro[1], Shenela Lakhani[13], Eric J. Mallack[13], Timothy Blake Palculict[14], Hong Li[15], Guojun Zhang[15,16], Faisal Zafar[17], Nuzhat Rana[17], Noriko Takashima[18], Hayato Matsunaga[19], Claudia Manzoni[20], Pasquale Striano[6,7], Mark F. Lythgoe[5], Jun Aruga[18,19]* and Wei Lu[3]* and Henry Houlden[1]* for the Synaps Study Group

[1]Department of Neuromuscular Disorders, University College London (UCL) Queen Square Institute of Neurology, London, United Kingdom, [2]U.O.C. Genetica Medica, Istituto di Ricovero e Cura a Carattere Scientifico (IRCCS) Istituto Giannina Gaslini, Genoa, Italy, [3]Synapse and Neural Circuit Research Section, National Institute of Neurological Disorders and Stroke, National Institutes of Health, Bethesda, MD, United States, [4]Department of Biological Sciences, International Islamic University Islamabad, Islamabad, Pakistan, [5]Centre for Advanced Biomedical Imaging, Division of Medicine, University College London, London, United Kingdom, [6]Department of Neurosciences, Rehabilitation, Ophthalmology, Genetics, Maternal and Child Health, Università Degli Studi di Genova, Genoa, Italy, [7]Pediatric Neurology and Muscular Diseases Unit, Istituto di Ricovero e Cura a Carattere Scientifico (IRCCS) Istituto Giannina Gaslini, Genoa, Italy, [8]Centre for Omic Sciences, Islamia College Peshawar, Peshawar, Pakistan, [9]School of Pharmacy, University of Reading, Reading, United Kingdom, [10]Department of Mathematics and Statistics, University of Reading, Reading, United Kingdom, [11]Department of Radiology, Great Ormond Street Hospital, London, United Kingdom, [12]Developmental Neurosciences Department, University College London (UCL) Great Ormond Street Institute of Child Health, London, United Kingdom, [13]Center for Neurogenetics, Feil Family Brain and Mind Research Institute, Weill Cornell Medicine, New York, NY, United States, [14]GeneDx, Gaithersburg, MD, United States, [15]Department of Human Genetics, Emory University School of Medicine, Atlanta, GA, United States, [16]Department of Pediatric Neurology, Children's Healthcare of Atlanta, Atlanta, GA, United States, [17]Department of Pediatrics, Multan Hospital, Multan, Pakistan, [18]Laboratory for Behavioral and Developmental Disorders, RIKEN Brain Science Institute (BSI), Saitama, Japan, [19]Department of Medical Pharmacology, Nagasaki University Institute of Biomedical Sciences, Nagasaki, Japan, [20]School of Pharmacy, University College London, London, United Kingdom

This study reports on biallelic homozygous and monoallelic *de novo* variants in *SLITRK3* in three unrelated families presenting with epileptic encephalopathy associated with a broad neurological involvement characterized by microcephaly, intellectual disability, seizures, and global developmental delay. *SLITRK3* encodes for a transmembrane protein that is involved in controlling neurite outgrowth and inhibitory synapse development and that has an important role in brain function and neurological diseases. Using primary cultures of hippocampal neurons carrying patients' SLITRK3 variants and in combination with electrophysiology, we demonstrate that recessive variants are loss-of-function alleles. Immunostaining experiments in HEK-293 cells showed that human variants C566R and E606X change SLITRK3 protein expression patterns on the cell surface, resulting in highly accumulating defective proteins in the Golgi apparatus. By analyzing the development and phenotype of SLITRK3 KO (*SLITRK3*$^{-/-}$) mice, the study shows evidence of enhanced susceptibility to pentylenetetrazole-induced seizure with the

appearance of spontaneous epileptiform EEG as well as developmental deficits such as higher motor activities and reduced parvalbumin interneurons. Taken together, the results exhibit impaired development of the peripheral and central nervous system and support a conserved role of this transmembrane protein in neurological function. The study delineates an emerging spectrum of human core synaptopathies caused by variants in genes that encode SLITRK proteins and essential regulatory components of the synaptic machinery. The hallmark of these disorders is impaired postsynaptic neurotransmission at nerve terminals; an impaired neurotransmission resulting in a wide array of (often overlapping) clinical features, including neurodevelopmental impairment, weakness, seizures, and abnormal movements. The genetic synaptopathy caused by SLITRK3 mutations highlights the key roles of this gene in human brain development and function.

KEYWORDS

SLITRK3, GABAergic synapse development, epilepsy, global developmental delay, inhibitory synaptic transmission, NGS - next generation sequencing

Introduction

Synapse development is a multi-step process coordinated by various molecules acting in a highly spatially and temporally controlled manner (de Wit and Ghosh, 2016). Synaptic cell adhesion molecules (CAMs) are an example of such molecules essential for the establishment and maturation of synaptic connections. Recent studies have identified a growing number of synaptic CAMs such as slit and NTRK-like family proteins (Slitrks) that are single-passing transmembrane proteins and bind to presynaptic protein tyrosine phosphatase (Ko, 2012; Yim et al., 2013; Won et al., 2019). Members of the Slitrk family contain twelve N-terminal leucine-rich repeat (LRR) domains and C-terminal regions that share homology with neurotrophin receptors (Aruga and Mikoshiba, 2003). They are expressed predominantly in neural tissues of the central nervous system and have neurite-modulating activity (Aruga et al., 2003; Aruga and Mikoshiba, 2003). Even though such molecules are involved in various stages of synapse development, their function diversity remains largely unclear.

Recent studies in humans and genetic mouse models have led to the identification of Slitrk family member genes as candidate genes that may be involved in the development of neuropsychiatric conditions such as obsessive-compulsive spectrum disorders, schizophrenia, Tourette syndrome, or trichotillomania (Proenca et al., 2011; Kang et al., 2016). Additionally, Slitrk3 abnormality has also been strongly associated with multiple cancers, such as human epithelial ovarian cancer (Wang et al., 2015) and squamous cell lung cancer (Bollig-Fischer et al., 2021).

SLITRK3 (Slit and Trk-like family member 3) is a synaptic cell adhesion molecule highly expressed at inhibitory synapses and enhances inhibitory synapse formation (Takahashi et al., 2012; Yim et al., 2013). Recent studies have provided additional evidence, furthering understanding of the mechanisms of GABAergic synapse formation by revealing a direct extracellular protein-protein interaction between SLITRK3 and another inhibitory postsynaptic cell-adhesion molecule, Neuroligin 2 (NL2) (Li et al., 2017) and the critical role of the SLITRK3-gephyrin interaction in the stabilization of pre- and post-synaptic compartments during development (Gomez-Castro et al., 2021). Collectively, these studies have shown that SLITRK3, through its extracellular domain, selectively regulates inhibitory synapse development via the trans-synaptic interaction with presynaptic cell adhesion molecule, receptor protein tyrosine phosphatase δ (PTPδ), the *cis* interaction with postsynaptic NL2, and the intracellular interaction with gephyrin. In this way, they exert differential, sometimes cooperative effects on GABAergic synapse formation depending on the developmental stage of the system. Furthermore, other recent studies have shown the critical role of a conserved tyrosine residue, Y969, in SLITRK3 carboxyl-terminus in GABAergic synapse development (Li et al., 2019; Gomez-Castro et al., 2021), indicating SLITRK3 may mediate signaling through both extracellular and intracellular domains.

In the brain, many types of interneurons make functionally diverse inhibitory synapses into principal neurons. In the mammalian brain, GABAergic synapses provide an important level of inhibitory balance to glutamatergic excitatory drive, therefore, controlling neuronal excitability and synaptic plasticity. As GABAergic inhibition is important in almost every aspect of brain physiology, and the dysregulation of GABAergic synapse development has been implicated in neurological and neuropsychiatric disorders (Ramamoorthi and Lin, 2011; Ko et al., 2015; Linde and Zimmer-Bensch, 2020; Cherubini et al., 2021), it is critical to understand the molecular determinants of GABAergic synapse formation. Prevention and treatment of brain disorders will also depend partly on the restoration of GABAergic function and/or inhibitory/excitatory balance.

In this study, we report on biallelic and monoallelic variants in *SLITRK3* in three families presenting with epileptic encephalopathy associated with neurodevelopmental findings that include seizures, motor delay, microcephaly, hyperactivity, and MRI brain abnormalities. Using primary cultures of

hippocampal neurons carrying patients' *SLITRK3* variants and in combination with electrophysiology, we characterized the functional effects of these variants on inhibitory synapses. By analyzing the development and phenotype of SLITRK3 KO (*SLITRK3*$^{-/-}$) mice, we further examined survival, seizure susceptibility, and any developmental deficits to correlate to the patients' phenotypes.

Materials and methods

After local institutional review board approval of this study and informed consent was provided by the families, we collected blood samples from the three patients and their parents and extracted DNA using standard procedures. Other families were identified by screening genomic data sets from several diagnostic and research genetic laboratories internationally, as well as using GeneMatcher (Sobreira et al., 2015).

Exome sequencing

To investigate the genetic cause of the disease, WES was performed in the three affected siblings (**Figure 1A**, II-1, II-2, II-3) as described earlier (Efthymiou et al., 2019) and analysis was carried out to fit a recessive model (i.e., homozygous or compound heterozygous), and/or located in genes previously associated epilepsy or other neurological phenotypes. The candidate variants were confirmed after filtering and interpretation according to the American College of Medical Genetics and Genomics/Association for Molecular Pathology guidelines (Richards et al., 2015) and segregation analyses were carried out using Sanger sequencing. Homozygosity mapping was performed on the genetic data from the 3 affected individuals and unrelated healthy controls age- and ethnically-matched (Quinodoz et al., 2021).

Genomic DNA from the submitted specimens were analyzed at GeneDx and enriched for the complete coding regions and splice site junctions for most genes of the human genome using a proprietary capture system developed by GeneDx for NGS with CNV calling (NGS-CNV). Using a custom-developed analysis tool (XomeAnalyzer), data were filtered and analyzed to identify sequence variants and most deletions and duplications involving three or more coding exons.

Molecular cloning

SLITRK3 constructs were cDNA synthesized by Genescript (USA) into pCMV-3Tag-4A by replacing the CDs for these inserts by using restriction enzymes *Bam*HI and *Xho*I (NEB), giving rise to all SLITRK3 plasmid variants. The variants generated were pCMV_SLITRK3[WT], pCMV_SLITRK3[E606X], and pCMV_SLITRK3[C566R]. Three Myc epitopes were then inserted before the stop codon into the three plasmids with the QuickChange Site-Directed Mutagenesis Kit (Agilent Technologies) to get SLITRK3-WT-Myc, SLITRK3-C566R-Myc, and SLITRK3-E606X-Myc plasmids.

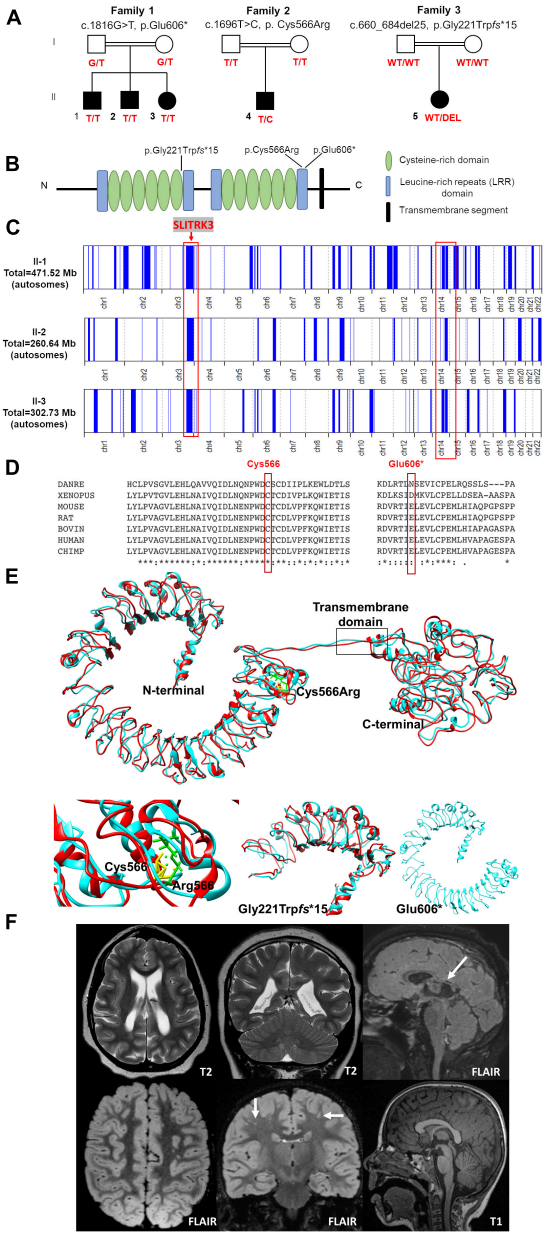

FIGURE 1
Pedigrees and genetic findings of the families carrying biallelic *SLITRK3* variants. **(A)** Pedigrees and segregation results (°+ represents the presence of the variant) of the three families **(B)** A schematic representation of the SLITRK3 protein showing the position of all variants identified. **(C)** Overview of the whole regions of homozygosity (ROH) in the exome of each affected individual in family 1. The region of homozygosity surrounding the SLITRK3 variant is indicated in the red bracket on the left. **(D)** Inter-species alignment performed with Clustal Omega shows the complete conservation down to invertebrates of the amino acid residues affected by the substitutions. **(E)** Predicted tertiary structure and homology models of the wild type (cyan) SLITRK3 protein using I-TASSER Structure Prediction server together with the mutated (red) c.1696T > C, p.Cys566Arg variant (top) with a disrupted disulfide bridge resulting in altered protein structure confirmation (bottom left), the frameshift variant c.660_684del25, p.Gly221Trp*fs**15 showing the presence of only a chunk of the extracellular domain being formed (bottom middle) and the nonsense c.1816G > T, p.Glu606Ter variant showing a shorter protein resulting in the termination of the chain and loss of the cytoplasmic domain of the protein (bottom right). **(F)** Radiological

(Continued)

FIGURE 1 (Continued)
findings; top panel (patient 5): Note the loss of white matter in both cerebral hemispheres with scalloping of the ventricular margins. On the sagittal FLAIR sequence, thinning of the posterior aspect of the corpus callosum is noted (arrow). Appearances would be compatible with periventricular leukomalacia in the context of white matter injury of prematurity, below panel (patient 4): Multiple tiny foci of white matter signal abnormality are observed in the subcortical white matter of both cerebral hemispheres. This is shown best on the coronal FLAIR image (arrows). The midline sagittal T1 is normal.

Western blotting

For plasmid validation, SLITRK3-WT-Myc, SLITRK3-C566R-Myc, or SLITRK3-E606X-Myc were transfected in HEK-293T cells using a calcium phosphate transfection reagent. Protein concentration in the soluble cell lysate supernatant was quantified with the standard BCA method. An equal amount of loading samples was mixed with an equal volume of 2x SDS loading buffer and boiled for 5 min at 95°C and then separated using pre-casted 10% SDS-PAGE gels (BioRad). The proteins were transferred onto PVDF membranes, blocked, and incubated with primary antibodies as: rabbit polyclonal anti-SLITRK3, (Proteintech, Cat#: 21649-1-AP), recognizing SLITRK3 C-terminus, rabbit monoclonal anti-Myc [(71D10), Cell Signaling Technology, Cat#: 2278], and mouse anti-α-Tubulin (Sigma, Cat#: T8203) overnight at 4°C. The PVDF membranes were then washed three times with 0.1% TBST and incubated with HRP-conjugated secondary antibodies for 1 h at RT. Protein was detected with the standard enhanced chemiluminescence (ECL) method.

Dissociated hippocampal neuronal culture

Dissociated cultures of hippocampal neurons were prepared as described previously (Gu et al., 2016; Li et al., 2017; Han et al., 2019). Briefly, timed-pregnant mice at E17.5−18.5 were anesthetized on ice and decapitated. The fetal hippocampi were quickly dissected out in ice-cold Hank's balanced salt solution, triturated with a sterile tweezer, and digested with papain (Worthington, LK003176) solution at 37°C for 30 min. After 5 min centrifuging at 800 rpm, the pellet was resuspended in Dnase I containing Hank's solution at room temperature (RT). It was then mechanically dissociated into single cells by gentle pipetting up and down. Cells were then transferred into Hank's solution mixed with trypsin inhibitor (10 mg/ml, Sigma, T9253) and BSA (10 mg/ml, Sigma, A9647), and centrifuged at 800 rpm for 10 min. The pellet was resuspended in neurobasal plating media with 2% fetal bovine serum (FBS) (Gibco, 10437-028), 2% B27 supplements, and L-glutamine (2 mM). Neurons were plated at a density of ~0.9×10^5 cells/well on poly-D-lysine (Sigma, P6407) pre-coated glass coverslips (12 mm) residing in 24-well plates for electrophysiological recording and immunocytochemistry. Culture media were changed by half volume with neurobasal maintenance media containing 2% B27 (GIBCO, 17504-044) supplements and L-glutamine (2 mM) once a week.

Electrophysiology in neurons

For the miniature inhibitory postsynaptic currents (mIPSC) recording, SLITRK3-WT-Myc, SLITRK3-E606X-Myc, or SLITRK3-C566R-Myc together with pCAGGS-IRES-GFP (SLITRK3:GFP = 9:1) were transfected into cultured hippocampal neurons at DIV 14-15 using Lipofectamine 3000 (ThermoFisher, L3000015). The coverslips were transferred to a submersion chamber on an upright Olympus microscope 48 h after transfection. They were perfused with aCSF solution supplemented with TTX (0.5 μM) and DNQX (20 μM) in an external solution (in mM): 140 NaCl, 5 KCl, 2 $CaCl_2$, 1 $MgCl_2$, 10 HEPES, and 10 D-glucose, adjusted to pH 7.4 with NaOH with 5% CO_2. GFP fluorescent positive and negative neurons were identified by epifluorescence microscopy. Neurons were voltage-clamped at −70 mV for the detection of mIPSC events. The internal solution for mIPSC recording (in mM): $CsMeSO_4$ 70, CsCl 70, NaCl 8, EGTA 0.3, HEPES 20, MgATP 4, and Na_3GTP 0.3. Osmolality was adjusted to 290−295 mOsm and pH was buffered at 7.25–7.35. Series resistance was monitored and not compensated, and cells in which series resistance varied by 25% during a recording session were discarded. Synaptic responses were collected with a Multiclamp 700B amplifier (Axon Instruments, Foster City, CA, United States), filtered at 2 kHz, and digitized at 10 kHz. All recordings were performed at RT. A total of 100–300 consecutive miniature events were semi-automatically detected by off-line analysis using customized software Igor Pro (Wavemetrics) using a threshold of 6 pA. All mIPSC events were visually inspected to ensure that they were mIPSCs during analysis, and non-mIPSC traces were discarded. All pharmacological reagents were purchased from Abcam, and other chemicals were purchased from Sigma.

Immunocytochemistry

The immunocytochemistry procedure in neurons was performed as described previously (Li et al., 2019). The indicated plasmids [SLITRK3-WT-Myc, SLITRK3-E606X-Myc or SLITRK3-C566R-Myc together with pCAGGS-IRES-GFP (SLITRK3:GFP = 9:1)] were transfected into cultured hippocampal neurons at DIV 14-15 using Lipofectamine 3000 (ThermoFisher, L3000015). After 48 h, the transfected cells grown on coverslips were gently rinsed with 1x PBS and fixed with 4% paraformaldehyde (PFA) and 4% sucrose in 1x PBS solution for 15 min at RT, followed by permeabilization with 0.2% TritonX-100 in 1x PBS for 15 min. Neurons were subsequently blocked with 5% normal goat serum in 1x PBS for 1 h and then incubated with primary antibodies as follows: anti-GFP (Cell signaling, #2555S, R), anti-Gephyrin (1:500, 147018, Synaptic Systems), and anti-vGAT (1:500, 131004, Synaptic Systems) in 1x PBS solutions overnight at 4°C. Cells were washed three times with 1x PBS and then incubated with Alexa Fluor 488, 555, or 647-conjugated IgG for 1 h. Coverslips were washed three times with 1x PBS and mounted with Fluoromount-G (Southern Biotech) for imaging acquisition.

For the surface immunostaining of HEK-293 cells transfected with HA-Neuroligin2 (HA-NL2) and SLITRK3-WT-Myc, SLITRK3-C566R-Myc, or SLITRK3-E606X-Myc, we used calcium

phosphate transfection to introduce DNA to these HEK cells. A transfection ratio of 1:1 (HA-NL2:ST3-Myc plasmid) was used. Briefly, HEK-293 cells were passed and planted in 24-well cell culture plates precoated with PDL (10 ug/ml). The next day, HEK cells were transfected with HA-NL2 + SLITRK3-WT-Myc, HA-NL2 + SLITRK3-C566R-Myc, or HA-NL2 + SLITRK3-E606X-Myc using a calcium phosphate transfection reagent (Takara bio.: 631312) for 40 h in a 37°C incubator. For the surface immunostaining, a dilution ratio of 1:100 anti-HA (rabbit, H6908, EMD Millipore) was diluted in the cell culture media [445 ml DME-H21, 5 ml Penicillin-Strep (100x), and 50 ml heat-inactivated FBS] and warmed up in 37°C dry bead bath for 10 min. Afterward, the coverslips containing transfected cells were gently picked from a 24-well plate and put on the autoclaved plastic board. Add an 80–100 ul antibody solution on the coverslips and incubate the board in a 37°C incubator for 30 min. Then, these coverslips were washed 1x PBS at room temperature (RT), followed by a fixation using 4% PFA + 4% sucrose in 1x PBS. The fixed cells were then incubated with mouse anti-Myc antibody (1:1000, 05-419, EMD Millipore) or rabbit anti-NL2 (1:500, 129508, SYSY) in 1xPBS containing 5% NGS and 0.3% Triton-X100 overnight.

For the immunostaining of the Golgi marker and total Myc, the transfected cells (after a 40-hr transfection period) were directly fixed in 4% PFA + 4% sucrose in 1x PBS. The fixed cells were then incubated with GM130 (Invitrogen, 703794, rabbit, 1:500) and mouse anti-Myc antibody (1:1000, 05-419, EMD Millipore) in 1xPBS containing 5% NGS and 0.3% Triton-X100 overnight. The next day, the coverslips were washed 3 × 10 min with 1x PBS before being incubated with Alexa-conjugated secondary antibodies (ThermoFisher, 1:1000) for 1 h at RT. After washing, coverslips were gently mounted with prolonged Glass antifade mountant with NucBlue (Invitrogen, P36985).

Image acquisition and analysis

Fluorescence images were acquired with a Zeiss LSM 880 laser scanning confocal microscope using a 63x oil-immersion objective lens (numerical aperture 1.4). For gephyrin puncta density analysis, confocal images from 1 to 3 secondary or tertiary dendrites (35 μm in length) per neuron from at least ten neurons in each group were collected and quantified by counting the number of puncta per 10 μm dendrites with ImageJ puncta analyzer program. Thresholds were set at 3 SDs above the mean staining intensity of six nearby regions in the same visual field. Thresholded images present a fixed intensity for all pixels above the threshold after having removed all of those below. Labeled puncta were defined as areas containing at least four contiguous pixels after thresholding.

For the co-localization experiments in HEK-293 cells, multiple z sections (7 optical slices) were acquired at 0.39 μm intervals. A 512 × 512-pixel screen was used to collect multiple z sections of secondary apical dendrites at 1.0–1.5 μm intervals. Images were taken using a 1024 × 1024-pixel screen for HEK cells, and the gains for the fluorophores were set between 700 and 800. The pinhole was set to 1 airy unit for all experiments. The scan speed function was set to 8, and the mean of 4 lines with double directions was applied. Laser power, digital gain, and offset settings were identical in each experiment using the "reuse" function in LSM software. We used Zeiss ZEN software to make maximal projection images from 7 serial optical sections for quantitative immunostaining analysis in HEK cells.

For the colocalization analysis of images of HEK-293 cells co-transfected with HA-NL2 and SLITRK3-Myc plasmids, we used the coloc2-plugin of the extended ImageJ version Fiji, and Pearson's *R* value was computed as indicated. The signal intensities of surface HA-NL2 to total NL2 in HEK cells were measured by ImageJ. A one-way ANOVA was analyzed, followed by Dunnett's multiple comparisons test with GraphPad Prism 10.0.

Animal experiments

All animal experiments were approved by Animal Experiment Committees at the RIKEN Brain Science Institute and the Animal Care and Use Committee of Nagasaki University. They were conducted following the guidelines for animal experimentation at RIKEN and Nagasaki University. For Slitrk3^{-} allele mice, Slitrk3 protein-coding region was replaced by a single LoxP sequence as described earlier (Takahashi et al., 2012). Same-sex litter mates were housed together with two to four mice per cage. All mice were maintained on a regular diurnal lighting cycle (12:12 light:dark) with *ad libitum* access to food (CE-2, CLEA Japan) and water. Cellulose bedding material (SAFE comfort natura, Oriental Yeast, Japan) was used as bedding. The sample sizes for each experiment were determined such that the power and significance in the two-sided test were 80 and 5%, respectively. However, the number of samples from the animals was minimized empirically. Control groups consisted of littermates of the same sex. One or two litters were reared in a cage. The total number of mice and cages allocated to each experiment are summarized in **Supplementary Table 1**. Behavioral, MRI, and interneuron analyses were carried out using B6N1/N2 mice. No inclusion/exclusion criteria were set before the study. All data were collected according to the randomly defined order of genotyping (tail cut). Potential confounders were not controlled. All animal experiments were carried out by experimenters who were blinded to animal identity. We did not set humane endpoints for maintaining the animal colony because some mice died suddenly.

Behavioral analysis

Adult male Slitrk3 KO (*Slitrk3*^{TM1Jaru}/*Slitrk3*^{TM1Jaru}, *Slitrk3*$^{-/-}$) and WT mice (*Slitrk3*$^{+/+}$, 8–32-week-old, littermates from mated heterozygotes) were used for behavioral tests. Male mice were used to avoid the effects of estrous cycles on behavioral phenotypes in females (Meziane et al., 2007). Mice were housed in a 12:12 h light-dark cycle, with the dark cycle occurring from 20:00 to 8:00, and behavioral experiments were carried out between 10:00 and 17:00. Please see **Supplementary Data** for a description of these behavioral experiments.

Magnetic resonance imaging (MRI) based volumetric analysis

Magnetic resonance imaging (MRI) images of the adult male mice were acquired by subjecting anesthetized mice to an MRI

scan using a vertical bore 9.4-T Bruker AVANCE 400WB imaging spectrometer (Bruker BioSpin, Rheinstetten, Germany). Animals were anesthetized with 3 and 1.5% isoflurane in air (2 L/min flow rate) for induction and maintenance, respectively. MRI images were obtained using the FISP-3D protocol of Paravision software 5.0, setting the following parameter values: Effective TE, 4.0 ms; TR, 8.0 ms; Flip angle, 15 degree; Average number, 5; Acquisition Matrix, 256 × 256 × 256, FOV, 25.6 × 25.6 × 25.6 mm. Regional volumetric changes were measured by tensor-based morphometry (Powell et al., 2016). The images were subjected to non-uniformity correction and intensity standardization, before a multi-iteration group-wise registration, including 5 iterations of affine registration and 3 iterations of non-rigid registration, was performed. The Jacobian determinant for each voxel, which indicates its relative expansion or contraction as a result of the transformation, was derived from the deformation fields from the final round of non-rigid registration. This was followed by voxel wise two-tailed *t*-tests using a general linear model to compare the KO and WT groups, with total brain volume as a covariate. Non-uniformity correction (Tustison et al., 2010) and image registration were performed using NifTK software (Clarkson et al., 2015). Intensity standardization (Nyul et al., 2000) and statistical analysis were performed using custom MatLab scripts.

Interneuron counting

Mice were anesthetized with inhalation of isoflurane. Cardiac perfusion was performed with 4% paraformaldehyde and 0.1 M sodium phosphate (pH 7.4). Excised brains were fixed in the same fixative for 4 h at room temperature with gentle agitation. Tissue blocks were cryoprotected with 20% sucrose in PBS at 4°C overnight and frozen in OCT compound (Sakura Finetek). Cryosection was performed using a CM3050 cryostat (Leica Biosystems) at a thickness of 12 μm. After sectioning, sections were immersed in PBS(-) for 5 min, followed by 0.3% hydrogen peroxide in methanol for 10 min at room temperature. After immersion in PBS(-), the sections were blocked with 1% skim milk (Difco), 2% normal goat or donkey serum and 0.1% Triton X-100 in PBS (-) at room temperature for 1 h and reacted with mouse anti-parvalbumin monoclonal antibody (Sigma-Aldrich, P3088, 1:4000), goat anti-somatostatin antibody (Santa-Cruz, SC7819, 1:250), or sheep anti-neuropeptide Y antibody (Millipore, AB1583, 1:500) at 4°C for 0.5–2.5 days. The bound antibody was detected by VECTASTAIN Elite ABC kits (Vector Laboratories) and 3,3′-diaminobenzidine (DOJINDO). For the immunostaining using anti-somatostatin antibody or anti-neuropeptide Y antibody, the sections were autoclaved (105 C for 5 min) in 10 mM sodium citrate (pH 6.0) before the peroxidase-methanol treatment for antigen retrieval. Images were acquired with an NDP slide scanner (Hamamatsu Photonics). For quantitative analyses, all stained images were taken with the same settings and manually counted by observers who were blinded to the genotypes.

Protein-protein network analysis

Protein-protein interaction (PPI) collection using STRING: The interacting proteins with the SLITRK3 was constructed using the STRING server[1] to identify both known and predicted protein-protein interactions. The network parameters (clusters, hubs, cliques and communities) were utilized to analyze the PPI network. The clusters, and groups of interacting proteins (nodes) in the network were calculated. SLITRK3 was used as the seed in the construction of a protein-protein network to identify proteins that might be involved in the interaction visualized by STRING and Cytoscape v.3.9.1 (Shannon et al., 2003). The SLITRK3 node is the query and the remaining nodes are relevant proteins that have the most connectivity with the query protein in the network of 11 proteins. In the bilateral network, the "nodes" represent the protein targets and "edges" represent the interactions of proteins.

Protein-protein interactions (PPI) collection using PINOT, filtering, and visualization of networks: The direct interactors of SLITRK3 were collected through PINOT (Tomkins et al., 2020) on 1/11/2022 (Settings: Organism: Homo sapiens; Filter level: Stringent). Because data were limited, all interactions were retained. In addition, even though manual curation by experts produces data in which we can have higher confidence compared to other methods, e.g., text mining, it is also time-consuming, potentially leading to delays in the inclusion of recently published data. We therefore performed manual curation of the literature (by querying SLITRK3 in PubMed on 26/8/2022) in order to extend our list of PPIs. This resulted in the identification of 4 additional interactions, of which only 1 was between two human proteins (i.e., NTRK3), while the rest were mouse proteins (i.e., Ptprd, NL2), and the first were considered of higher confidence. The second layer interactome of SLITRK3 was built based on the results from PINOT and the high confidence interactors from the manual curation, using PINOT on 1/11/2022 (Settings: Organism: Homo sapiens; Filter level: Stringent). From the indirect interactors of SLITRK3, only those with an FS higher than 2 were retained in the network. The PPINs were visualized using Cytoscape (v3.9.0) (Shannon et al., 2003).

Enrichment and grouping: The second layer SLITRK3 network was analyzed using enrichment through g:Profiler (Raudvere et al., 2019) on November 2, 2022 (version e107_eg54_p17_bf42210) (Settings: Statistical domain scope: Only annotated genes; Significance threshold: Bonferroni correction, User threshold: 0.05, No electronic GO annotations). The top resulting Gene Ontology Biological Process (GOBP) terms based on the adjusted *p*-value, as calculated by g:Profiler, were selected based on the distribution of the *p* values, as shown in **Supplementary Figure 4D** (n = 125). The significant GOBP terms were grouped into semantic classes based on semantic similarity using the in-house dictionaries of the Manzoni lab (Tomkins et al., 2020). The semantic classes were grouped further into functional groups. The functional groups named General and Metabolism were not included in the analysis, as done previously (Vavouraki et al., 2021). Neuronal-related terms were observed in multiple functional groups, so text mining using the keys "nerv," "neur," "brai," and "synap," were used to identify these terms in our results. The calculation of the enrichment ratios of the neuron-related words and the statistical analysis were calculated, as previously described (Vavouraki et al., 2021). The *p*-value was calculated using the Excel function: = 2*(1-NORM.DIST(x, mean, sd, TRUE)).

1 https://string-db.org/

Protein modeling of WT and mutant SLITRK3

There are currently no 3-D crystal structures of the SLITRK3 protein available, and no identified templates were found for comparative modeling. Therefore, the I-TASSER Structure Prediction server was used for predicting the protein tertiary structure (Yang et al., 2015), as described in the **supplementary materials**.

Results

Clinical findings

Family 1 consists of a 7-year-old boy (F1:II-1), a 6-year-old boy (F1:II-2), and a 5-year-old girl (F1:II-3) from a consanguineous family of Pakistani descent (parents are first cousins) (**Figure 1** and **Table 1**). Family history was unremarkable, except for one prior spontaneous miscarriage. The pedigree suggested an autosomal recessive inheritance. All presented with generalized tonic-clonic seizures since a young age (6 months for F1:II-1, 24 months for F1:II-2, and 18 months for F1:II-3) and extensor spasms in F1:II-2. No significant evolution of the epileptic phenotype emerged over time and seizures were controlled by antiepileptic drugs alone or in combination. All the patients developed progressive neurodevelopmental delay, with poor or absent speech and severe intellectual disability. F1:II-2 and F1:II-3 have short stature; 94 cm (<0.4th centile) and 84 cm (<0.4th centile), respectively. F1:II-3 also has microcephaly at 44 cm (<0.4th centile). EEG showed left parietal focal epileptogenic activity in F1:II-1 and diffuse encephalopathy in his two siblings. Ophthalmological examination in F1:II-1 showed retinal pigment epithelium abnormalities. Upon neurological examination, all three siblings presented with hyperactivity, whereas spasticity, brisk DTR, and moderate weakness were observed in F1:II-1 and F1:II-2. Brain MRI in F1:II-1 was unremarkable.

Family 2 consists of a 5-year-old boy (F2:II-1) of American origin (**Figure 1**). Pregnancy was complicated by intrauterine growth restriction (IUGR) but the child was born full term. He first presented with febrile seizures at 3 years of age accompanied by generalized fever (102F, 38.9 C) with stiffness, focal shaking, and limping, which lasted less than 1 min. Six months later he experienced tonic-clonic seizures with post-ictal symptoms. Since then, he experienced both febrile and non-febrile seizures, which manifested as generalized tonic-clonic episodes. Overnight video EEG at the age of 2 years showed background slowing, occasionally max left temporal, multifocal interictal epileptiform discharges (IEDs), max right central, often admixed with sleep architecture (**Supplementary Figure 1**). Seizures were controlled by Levetiracetam alone. Brain MRI at the age of 2 years showed multiple subcortical white matter T2-hyperintensities without enhancement or mass effect. These lesions were non-specific and the differential diagnosis was long including gliosis, demyelination, dysmyelination, Lyme, vasculitis, and chronic ischemia (**Figure 1F**). There was optic nerve head flattening suggestive of papilledema. There were no developmental concerns, and a motor skill assessment revealed no atrophy or fasciculation, but mild hypotonia was observed. Ophthalmology evaluated him and a dilated exam showed normal healthy optic nerves without any edema. The patient was alert and interactive, he made good eye contact and followed commands. Speech was fluent and language was appropriate for his age. Recent and remote memory were grossly intact.

Family 3 consists of a 16-year-old girl (F3:II-1) of African American origin (**Figure 1**). The pregnancy was complicated by IUGR but she was born full-term. Parents were concerned about motor delays very early on but became even more concerned around the age of 9−12 months. She was diagnosed with epilepsy, severe global developmental delay, and intellectual disability. She rolled over at 6 months but did not meet any other motor milestones until after 2 years old and she did not walk until 6 years old. She currently remains non-verbal and does not use signs; she communicates via vocalizations and walking to what she wants. She started having staring spells at around 9−12 months old. These progressed to generalized tonic-clonic seizures lasting up to 2 min with post-ictal symptoms. Seizures were controlled with Leviteracetam and Clonazepam. Her last seizure occurred at the age of 14.5 years. F3:II-1 has short stature (<0.4th centile), microcephaly at 47 cm (<0.4th centile), and dysmorphic features (larger ears, prominent nose, wide mouth, short philtrum, everted upper lip, camptodactyly, flat feet). She has also been diagnosed with cortical vision impairment and nystagmus. The mother reported significant behavioral issues including breath holding, difficulty staying asleep, teeth grinding, hand rubbing, laughing fits, and crying spells. Brain MRI at the age of 11 months showed mild ventricular enlargement and prominent sulci suggestive of decreased brain volume, thin corpus callosum, and an irregular border to the ventricular system, raising the possibility of periventricular leukomalacia (**Figure 1F**). A recent examination at 17 years of age revealed the development of secondary amenorrhea. Other clinical features included hypotonia and spasticity.

Further clinical details of the patients identified in our cohort can be seen in the **Supplementary Table**.

Genetic findings

In total, 83,572,847 (II-1) and 81,527,162 (II-2) unique reads were generated by WES for the 7-year-old (F1:II-1) and the 6-year-old (F1:II-2) of family 1. After applying the previously mentioned filtering criteria, no plausible shared compound heterozygous variants were identified by WES; there was, however, a gene carrying a novel (likely) pathogenic variant, according to ACMG variant interpretation guidelines (Richards et al., 2015) (**Table 2**), which was homozygous in all three probands in family 1 (**Figure 1**). A homozygous frameshift deletion in *SLITRK3* (NM_014926: c.1816G > T, p.Glu606*) emerged as the most likely explanation for the disease pathogenesis. This is also supported by the more severe impact of the mutation on protein function (truncating vs. missense) and an existing functional report previously linking cell adhesion molecules (CAM) such as SLITRK3 to synaptogenesis and GABAergic synapse development (Li et al., 2017). The variant was residing within the largest region of homozygosity (out of two) in all three affected individuals of family A (**Figure 1C**). Segregation

analysis performed by traditional Sanger sequencing confirmed the homozygous variant in the three affected siblings and heterozygous in both their parents. The identified *SLITRK3* homozygous variant was submitted to the Leiden Open Variation Database (; variant ID #0000693802).[2] Through clinical whole exome sequencing carried out at GeneDx, a *de novo SLITRK3* variant (c.1696T > C, p.Cys566Arg) was identified for family 2 and a *de novo* mosaic frameshift variant (c.660_684del25, p.Gly221Trp*fs**15) in family 3 (**Figure 1D**).

We further searched data from the 1,00,000 Genomes Project (Genomics England) (Turnbull et al., 2018) for families where affected individuals harbored monoallelic or biallelic variants in *SLITRK3*. All genomes from probands and affected family members (n = 15,790) recruited under the Neurology Disease group and Mitochondrial disorders in the 100KGP were annotated and analyzed for *SLITRK3* variants. Within this cohort, 2,638 individuals were recruited under the "Inherited Epilepsy Syndromes." After filtering the dataset for *de novo* variants, seven possible cases were identified. Weak phenotypic overlap and similarity across the seven hits led to the exclusion of these individuals from this cohort.

Molecular findings

We performed the Western blot assay using an anti-SLITRK3 antibody recognizing SLITRK3 C-terminus and an anti-Myc antibody to identify the expression pattern of SLITRK3-WT-Myc, SLITRK3-C566R-Myc, and SLITRK3-E606X-Myc in HEK-293T cells (**Figure 2A**). We found that the molecular weight of SLITRK3-C566R-Myc was slightly higher than WT. As the truncated form of the SLITRK3 mutant, For E606X, which is a nonsense mutation, leads to a loss of part of the transmembrane domain, and the entire C-terminus of SLITRK3 (**Figure 1B**). Indeed, using the SLITRK3 antibody, the E606X mutation could not be detected (**Figure 2A**). Thus, we probed the E606X mutant using an anti-Myc antibody and found that the SLITRK3-E606X mutation resulted in a truncating molecule with a lower molecular weight than the SLITRK3-WT protein.

To study the functional effect of these mutations on inhibitory synapses, we conducted the whole-cell recordings to measure miniature inhibitory postsynaptic currents (mIPSCs) in cultured hippocampal neurons (DIV14) overexpressing human WT-SLITRK3-Myc, SLITRK3-C566R-Myc or SLITRK3-E606X-Myc mutants (also simultaneously expressing GFP). In neurons overexpressing WT-SLITRK3, the frequency, but not amplitude, of mIPSCs was significantly increased (**Figures 2B–D**), similar to an early study (Li et al., 2019). In contrast, in neurons overexpressing SLITRK3-C566R, GABAergic transmission had no change compared with the control cells showing that the missense mutation of C566R essentially abolished the effect of SLITRK3 overexpression on GABAergic transmission (**Figures 2B–D**). In addition, the mIPSC frequency and amplitude had no change in neurons expressing SLITRK3-E606X mutant compared with the control cells (**Figures 2B–D**), suggesting that premature termination of SLITRK3 at E606 inactivates the function of SLITRK3 in promoting GABAergic transmission.

To further examine the role of human SLITRK3 mutants, we investigated the function of these mutants in the regulation of GABAergic synapses in hippocampal neuronal cultures, as SLITRK3 is a key inhibitory synaptic cell adhesion molecule. To this end, we over-expressed SLITRK3-WT-Myc, SLITRK3-C566R-Myc, or SLITRK3-E606X-Myc together with pCAGGs-IRES-GFP in dissociated hippocampal neurons, and examined the densities of vGAT and gephyrin, the inhibitory pre- and post- synaptic markers, respectively, in neuronal dendrites. The GFP expression pattern helped delineate the transfected neuronal dendrites. We found that both vGAT and gephyrin in neuronal dendrites were significantly increased in hippocampal neurons overexpressing SLITRK3-WT-Myc (**Figures 2E–G**), consistent with the recent study (Li et al., 2019). In contrast, overexpression of human SLITRK3 mutants of SLITRK3-C566R-Myc or SLITRK3-E606X-Myc did not change the densities of vGAT and gephyrin in neuronal dendrites (**Figures 2E–G**), showing that these two mutations abolish the ability of SLITRK3 in enhancing GABAergic synapse development.

Finally, to determine how the SLITRK3 human variants can affect the trafficking to the cell surface in heterologous cells, we used the C-terminal-tagged human SLITRK3 plasmids and mouse N-terminal-tagged HA-Neuroligin2 (HA-NL2) to co-express them individually in HEK-293 cells. We then performed immunocytochemistry (ICC) staining experiments to examine the expression pattern of WT and truncated or missense SLITRK3 mutants by measuring the ratio of surface HA-Neuroligin2 (HA-NL2), total SLITRK3-myc, and Golgi marker GM130. We found that the SLITRK3-E606X-Myc and SLITRK3-C566R-Myc variants changed the protein expression pattern at the cell surface, resulting in highly accumulating defective SLITRK3 protein in the Golgi apparatus (**Figures 3A–F**).

Animal studies

In a previous study, SLITRK3 KO mice were shown to have reduced inhibitory synapse density and to exhibit increased seizure susceptibility and abnormal epileptiform activity in electroencephalogram (Takahashi et al., 2012). However, we have not observed either spontaneous or handling-induced seizure-like behavioral abnormalities during their maintenance or behavioral tests. To better understand the biological role of SLITRK3, we analyzed the developmental behavior and phenotypes of SLITRK3 KO (*SLITRK3*$^{-/-}$) mice. During postnatal development, SLITRK3 KO mice exhibited incomplete lethality. Genotyping for the adolescent period indicated that 59% (B6N1/N2, KO mice generated in 129P2 strain background backcrossed to C57BL/6 strain once or twice) or 73% (B6N8, similarly backcrossed eight times) of the SLITRK3 KO mice died before 4 weeks-old. There was a significant difference in the genotype ratios between the B6N1/N2 group and the B6N8 group (P = 0.0095 in χ^2-test, **Table 3**), suggesting that the lethality was affected by the difference in genetic backgrounds. In the longitudinal analysis of B6N8 mice, 7 out of 9 SLITRK3 KO mice died on P20 or P21, and body weight was significantly lower than SLITRK3 WT both at 2 week-old (−29%, P = 0.0022) and 3 week-old stages (−45%, P = 0.00048)

2 www.lovd.nl/

10.3389/fnmol.2024.1222935

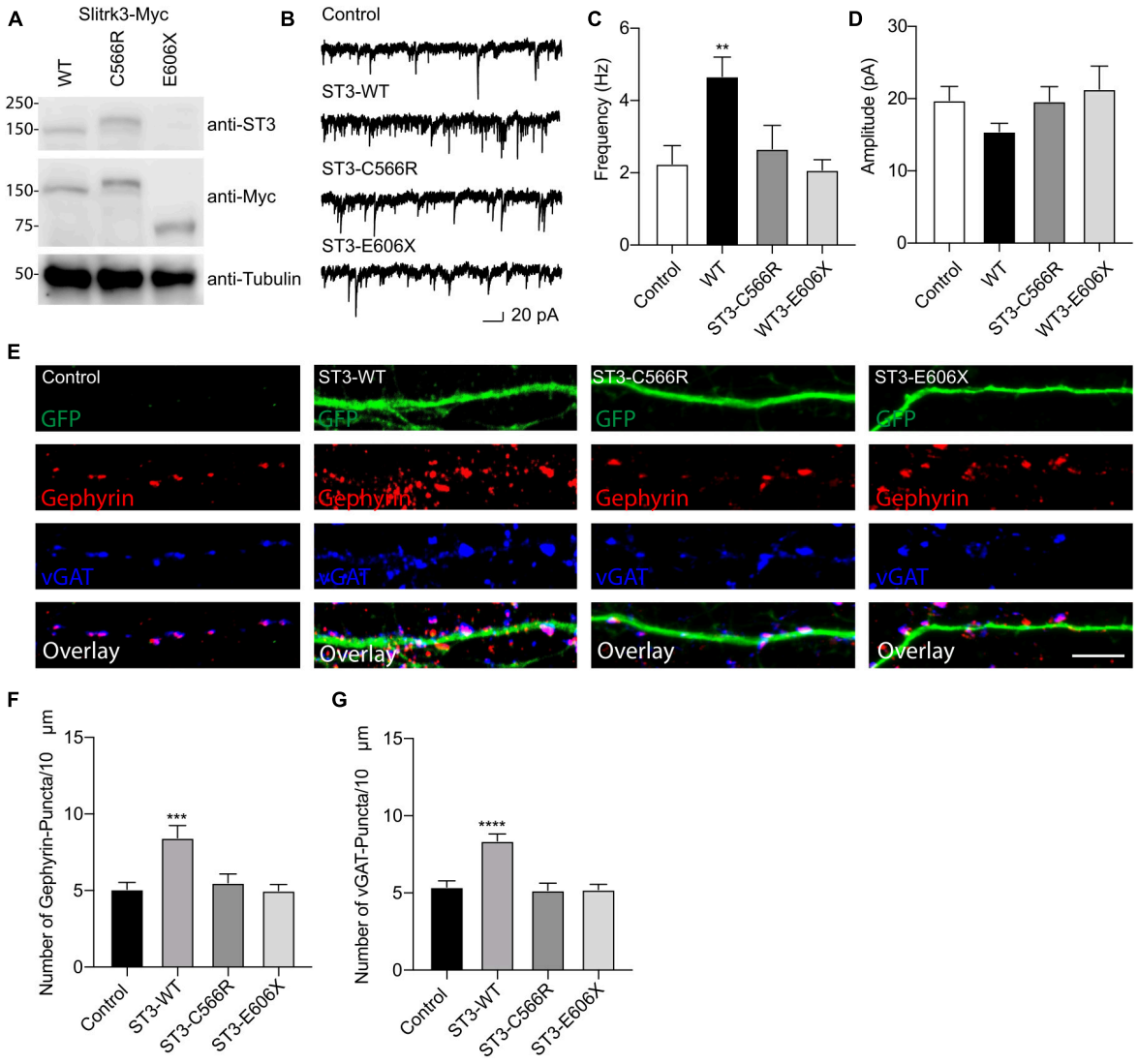

FIGURE 2
Functional effect of SLITRK3 variants on inhibitory synapses. **(A)** Identification of SLITRK3-WT, SLITRK3-C566R, and SLITRK3-E606X expression in HEK-293 cells. Cell lysates from HEK-293 cells transfected with SLITRK3-WT-Myc, SLITRK3-C566R-Myc, or SLITRK3-E606X-Myc were blotted with anti-SLITRK3, anti-Myc and anti-tubulin antibodies. *N* = 3 independent repeats. **(B–D)** Human mutants in SLITRK3 are essential for GABAergic synaptic transmission. mIPSC recording showed that overexpression of human WT- SLITRK3 significantly increased mIPSC frequency, whereas overexpression of the SLITRK3-C566R mutant had no effect on the frequency of mIPSCs in cultured hippocampal neurons. Insets showed the mean ± SEM of mIPSC frequency and amplitude [Frequency (Hz): Control, 2.25 ± 0.50, *n* = 10; WT- SLITRK3, 4.67 ± 0.54, *n* = 9; SLITRK3-C566R, 2.67 ± 0.65, *n* = 11; SLITRK3-E606X, 2.08 ± 0.28, *n* = 10. One-way ANOVA test, $^{**}p = 0.0058$; Mann-Whitney test, Control vs. SLITRK3-WT: $^{**}p = 0.004$; Control vs. SLITRK3-C566R: $p = 0.918$; Control vs. SLITRK3-E606X: $p = 0.579$. Amplitude (pA): Control, 19.770 ± 1.91, *n* = 10; SLITRK3-WT, 15.44 ± 1.14, *n* = 9; SLITRK3-C566R, 19.65 ± 2.02, *n* = 11; SLITRK3-E606X, 21.30 ± 3.22, *n* = 10. One-way ANOVA test, $p = 0.33$; Mann-Whitney test, Control vs. SLITRK3-WT: $p = 0.08$; Control vs. SLITRK3-C566R: $p = 0.76$; Control vs. SLITRK3-E606X: $p = 0.91$. *N* = 5–6] Scale bar, 20 pA and 1 s. *N* = 6 independent repeats. **(E–G)** Identification of C566R and E606X in SLITRK3 that is important for GABAergic synapse density in hippocampal neurons. Representative images of dendrites and quantification analysis showed that overexpression of human SLITRK3-WT significantly increased vGAT and gephyrin puncta density in cultured hippocampal neurons, whereas overexpression of human SLITRK3-C566R and SLITRK3-E606X, did not change vGAT or gephyrin puncta density [vGAT: Control: 5.38 ± 0.39, *n* = 19, SLITRK3-WT: 8.36 ± 0.44, *n* = 17, SLITRK3-C566R: 5.17 ± 0.46, *n* = 16, SLITRK3-E606X: 5.22 ± 0.33. One-way ANOVA test, $^{****}p < 0.0001$, F = 12.22; Mann-Whitney test, Control vs. SLITRK3-WT: $^{****}p < 0.0001$; Control vs. SLITRK3-C566R: $p = 0.62$; Control vs. SLITRK3-E606X: $p = 0.66$. Gephyrin: Control: 5.07 ± 0.45, *n* = 19, SLITRK3-WT: 8.44 ± 0.80, *n* = 17, SLITRK3-C566R: 5.50 ± 0.58, *n* = 16, SLITRK3-E606X: 5.00 ± 0.40. One-way ANOVA test, $^{***}p = 0.0001$, F = 8.038; Mann-Whitney test, Control vs. SLITRK3-WT: $^{**}p = 0.002$; Control vs. SLITRK3-C566R: $p = 0.68$; Control vs. SLITRK3-E606X: $p = 0.90$]. *N* = 4 independent repeats (SLITRK3 denoted as ST3 on figure).

(Figure 4). On the other hand, B6N1/N2 group mice did not show significant body weight gain even at adult stages (Figure 4). Adult SLITRK3 KO (B6N1/N2) mice are known to exhibit enhanced susceptibility to pentylenetetrazole-induced seizure and the appearance of spontaneous epileptiform EEG (Takahashi et al., 2012). However, we rarely observed either spontaneous or handling-induced seizure-like behavioral abnormalities during their maintenance or behavioral tests, and little is known about the other neurological abnormalities. We then investigated their behavioral abnormalities. As a result, SLITRK3 KO mice showed

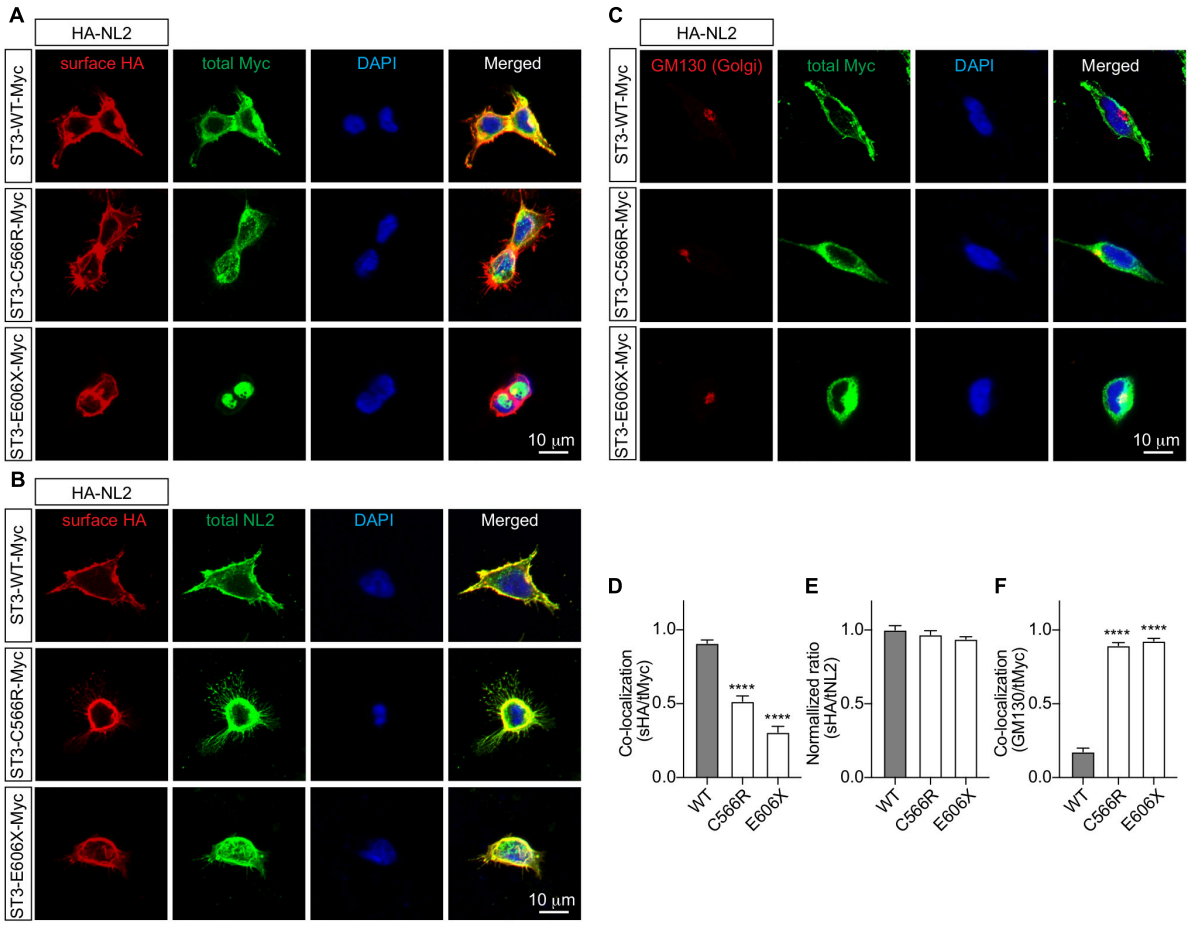

FIGURE 3
SLITRK3 C566 and E606 sites are necessary for surface expression of SLITRK3 in heterologous cells. **(A–C)**. Representative images of HEK-293 cells transfected with HA-NL2 and SLITRK3-WT-Myc, SLITRK3-C566R-Myc, or SLITRK3-E606X-Myc using the calcium phosphate transfection **(A, D)**. Immunostaining of surface (s) HA and total (t) Myc showed that SLITRK3-C566R-Myc and SLITRK3-E606X-Myc significantly reduced the colocalization ratio of sHA/tMyc compared with ST3-WT-Myc **(B, E)**. Immunostaining of sHA and total NL2 showed that SLITRK3-WT-Myc, SLITRK3-C566R-Myc, and SLITRK3-E606X-Myc did not change the sHA/tNL2 ratio in HEK cells **(C, F)**. Immunostaining of the total Golgi marker (GM130) and total Myc showed that SLITRK3-C566R-Myc and SLITRK3-E606X-Myc dramatically increased the colocalization ratio of GM130/tMyc. These results showed that human ST3 variants C566R and E606X changed SLITRK3 protein expression patterns on the cell surface, resulting in highly accumulating defective proteins in the Golgi apparatus. Colocalization analysis of images of HEK-293 cells **(A, C)** using the coloc2-plugin of the extended ImageJ version Fiji. Pearson's *R* value was computed as indicated (data represent mean ± S.E.M., $n = 10$, **** indicate a significant difference with $p < 0.0001$). A one-way ANOVA was analyzed, followed by Dunnett's multiple comparisons test with GraphPad Prism 10.0. The immunostaining intensities of surface HA-NL2 to total NL2 in HEK cells **(B)** were measured by ImageJ (data represent mean ± S.E.M., $n = 10$, **** indicate a significant difference with $p < 0.0001$). A one-way ANOVA was analyzed, followed by Dunnett's multiple comparisons test with GraphPad Prism 10.0. $N = 3$ independent experiments. Scale bar, 10 μm.

higher motor activities than WT littermates in several tests. In their home cages, higher spontaneous activities were observed both at light and dark phases (Figure 5A). On rotating rods, SLITRK3 KO mice stayed longer time at the first round of the tests (Figure 5B). On elevated plus maze apparatus, SLITRK3 KO mice moved longer distances (Figure 5C). In forced swimming, SLITRK3 KO mice showed less immobility (Figure 5D). The forced swimming test is often used to assess the effect of antidepressants. However, other behavioral tests used to assess mood-associated behaviors such as immobile time in tail suspension test or marble burying test did not show differences between WT and KO (Supplementary Figure 2).

Another characteristic feature included the increased open arm entries and falling from the elevated plus maze apparatus (Figure 5C) and decreased stay time in the wire-hanging test (Figure 5E). These signs were thought to reflect either reduced anxiety and/or impaired sensorimotor function to prevent falling off. There were no clear genotype differences in center-area stayed time in the open field test, which is an anxiety-related behavioral index (Figure 5F). On the other hand, we observed significant WT-KO genotype differences in some other sensorimotor function-related parameters such as increased freezing response after the first conditioned-unconditioned stimulus in the fear conditioning test and decreased auditory startle response to 95dB stimuli in the auditory startle response test (Supplementary Figure 2). Although the sensory modalities were different among the tests (i.e., vision-depth-height, nociception-foot-shock, auditory-noise), it seemed likely that SLITRK3 KO involves some sensory system dysfunction.

SLITRK3 KO mice also showed different responses to both inanimate and animate objects. In the case of an inanimate object

(a small cylinder) on an open-field apparatus, SLITRK3 KO mice showed fewer move episode counts than WT mice (Figure 5F). In the reciprocal social interaction test (resident-intruder test), SLITRK3 KO mice (resident) showed a lower approach to the anogenital region of the unfamiliar (intruder) mice (Figure 5G). In the social discrimination test, SLITRK3 KO mice showed fewer approaches to the cage with unfamiliar mice (Figure 5H).

Collectively, the behavioral abnormalities of SLITRK3 KO mice may be well categorized into context-dependent higher motor activities, sensorimotor function abnormalities, and altered responses to unfamiliar objects. We also summarize these abnormalities using broad terms such as cognitive dysfunction.

Because a previous study showed defective inhibitory synapse formation on hippocampal pyramidal neurons in SLITRK3 KO mice, we investigated interneuron numbers in the hippocampus. It was found that numbers of parvalbumin (PV)-positive interneurons were reduced in hippocampal CA1, CA3, and dentate gyrus regions (Figure 6A). On the other hand, the numbers of somatostatin-positive neurons and neuropeptide Y-positive neurons were comparable between the two genotypes (Figure 6A). We also quantified the PV-positive cell numbers in the somatosensory cortex. However, there were no clear genotype-dependent differences (Figure 6B). We also examined the gross morphology of SLITRK3 KO brains by MRI. The total brain volume was comparable between SLITRK3 WT and KO mice (Supplementary Figure 3). There were no clear genotype-dependent regional volume changes in tensor-based morphometry analysis (Supplementary Figure 3). These results indicated that SLITRK3 deficiency caused a selective reduction in the PV-positive interneuron subset.

Protein-protein interaction network analysis

As previously mentioned, a functional connection between SLITRK3 and synapses is outlined in earlier research (Li et al., 2017), which increased our confidence in identifying the association between the newly identified variant and the clinical phenotype. Due to there being limited functional studies of human SLITRK3 before this study, we performed protein-protein interaction network analysis combined with functional enrichment to study the functions associated with SLITRK3 based on its interactome before further investigating the variant.

Firstly, the protein-protein interactions (PPIs) of SLITRK3 were collected using STRING, which resulted in 11 potential interactors, including other important CAMs (i.e., NLGN2, NRXN2, PRPRS) (Supplementary Figure 4A). The subsequent functional enrichment analysis was based on a more stringent collection of PPIs. The first layer interactome included only human PPIs, using the online tool PINOT (n = 6 direct interactors), complemented by our in-house manual curation of the literature to include more recent PPIs potentially missing from the queried databases (n = 1 direct interactor). The seven interactors were used as seeds for the creation of the second layer interactome (i.e., interactions of the direct interactors of SLITRK3) (Supplementary Figures 4B, C) and analyzed further using enrichment of biological processes and pathways. The top resulting GOBP terms had similar themes related to phosphorylation, intracellular signal transduction, ERBB signaling pathway, MAPK cascade, response to stress, cellular localization, cell migration, epidermal growth factor receptor signaling pathway, positive regulation of immune system process, cell death, vesicle mediated transport, Fc receptor mediated stimulatory signaling pathway, receptor-mediated endocytosis, cell differentiation, cell adhesion, and apoptosis. Interestingly, neuron-related terms were also observed and their enrichment ratios and p values of enrichment were calculated for "*nerv*," "*neur*," and "*synap*" (2.90, 0.018; 1.40, 0.037; and 1.29, 5.6 × 10-9), providing an additional indication of the role of SLITR3 and its interactome in the function of neurons. Pathway enrichment analysis highlighted pathways that could be implicated with SLITRK3's physiological function, including signal transduction, cytokine signaling in the immune system, axon guidance, nervous system development, and clathrin-mediated endocytosis (Supplementary Tables 2, 3).

In silico structural modeling

The structural modeling of WT and mutant SLITRK3 proteins showed that, in the WT protein, the Cys556 residue forms a disulfide bridge with the Cys591 that is disrupted due to the heterozygous c.1696T > C, p.Cys566Arg variant. The mutated Arg566 residue forms an interaction with the vicinity residues involving the side chain. This results in disulfide bridge breaking and interaction of the Arg566 can alter the protein's structural confirmation. Overall, there is a similarity between WT and mutated structures but a significant position difference such as that of alpha helixes and β-sheets has been observed after running the energy minimization of these models. Nonsense variants such as the homozygous c.1816G > T, p.Glu606* are predicted to create a shorter protein, compared to normal SLITRK3, resulting in termination of the chain and loss of the cytoplasmic domain of the protein. Additional modeling of the frameshift mutation c.660_684del25, p.Gly221Trp*fs**15 with Chimera v.1.4. revealed the presence of only a chunk of the extracellular domain of the protein, which is predicted to impede the protein's normal function (Figure 1E).

Discussion

We identified *de novo* heterozygous and bi-allelic mutations in *SLITRK3* in 5 individuals from 3 families, with a developmental epileptic encephalopathy phenotype. The clinical picture was predominated by early onset global developmental delay, seizures, intellectual disability, and attention deficit–hyperactivity disorder, all of which pointed to a brain disorder. Early studies have shown that SLITRK3 is highly enriched at GABAergic inhibitory synapses and plays a critical role in the regulation of GABAergic synapse development (Takahashi et al., 2012; Yim et al., 2013). Recently, mechanistic investigations have demonstrated that SLITRK3 is involved in GABAergic synaptogenesis at the late stage of development (Li et al., 2017) and functions in adenosine receptor-mediated inhibitory synapse stabilization during development, a process depending on SLITRK3 Y969 (Li et al., 2019; Gomez-Castro et al., 2021). Our data have now revealed that epilepsy-associated human mutations in SLITRK3 disrupt its function

TABLE 1 Summary of the clinical features of SLITRK3 patients.

	Family 1			Family 2	Family 3
SLITRK3 variant (NM_014926.4)	c.1816G > T; p.(Glu606*)			c.1696T > C; p.(Cys566Arg)	c.660_684del25; p.(Gly221Trp*fs**15)
Inheritance/phase	Biallelic			*De novo*	*De novo*
Current age, gender	7y, M	6y, M	5y, F	5y, M	16y, F
Ethnicity	Pakistani			Montenegrian/Australian	African American
Consanguinity	+			No (but ROH on microarray)	No
History of miscarriages	+ (1)			1 miscarriage (first trimester)	No
Prenatal history	H/O HIE-I	insignificant	insignificant	Full-term, scheduled C-section	NA
Neonatal course	remain admitted for 2 days	Normal	Normal	Normal	NA
Short stature	+ (−2 SDS)	+ (−2 SDS)	+ (−2.7 SDS)	No	+ (−5.9 SDS)
Microcephaly	–	–	+ (−2.9 SDS)	No	+ (−5 SDS)
Dysmorphic features	–	–	–	–	larger ear, prominent nose, larger mouth, short philtrum, everted upper lip, camptodactyly in fingers, flat feet
Global DD/ID	+	+	+	–	+
Unassisted walk	+	+	+	+	+
Speech	Few words	Few words	Absent	Normal	Absent
Behavioral abnormalites	–	–	–	–	breath holding, difficulty staying asleep, teeth grinding, hand rubbing, laughing fits, and crying spells
Seizures	+	+	+	+	+
Type, onset	GTCS, 6m	GTS and ES, 2y	GTC, 18m	FS, 3y	staring spells, 9−12 m
Frequency	1−10/day	0−5/day	7−8/day	1/day	1/year, now seizure free for 1.5y
Duration	5 min	1−2 min	4−5 min	<1 min	1−2 min
Post-ictal status	++	++	–	+	+
Evolution	tonic-clonic	tonic-clonic, spasms	tonic-clonic	tonic-clonic	tonic-clonic
Status epilepticus	2 times	once	No	No	No
Trialled drugs	PB, VPA, LEV	VPA, LEV	LEV	LEV	LEV, CNZ
Response to treatment	Controlled	Controlled	Controlled	Controlled (last sz in 2018)	Controlled

(Continued)

10.3389/fnmol.2024.1222935

TABLE 1 (Continued)

	Family 1			Family 2	Family 3
EEG at last follow-up	Left parietal focal epileptogenic activity	Severe encephalopathy	Severe encephalopathy	Slowed background, right and left central and anterior slow and sharp waves; diffuse epileptic discharges	(1) diffuse slow spike slow waves, irregular slow spike-and-slow wave complexes (2) generalized paroxysmal fast activity prominent over the anterior regions. (3) Intermittent generalized delta activity. (4) Poorly organized and slowed background activity
Hypotonia	–	–	–	+, mild	+
Spasticity	-	+	-	-	+
Psychomotor regression	–	–	–	–	few words and signs by 12 m but lost all around 12 m
Opthalmological findings	RPE abnormalities	◦	◦	◦	cortical vision impairment
Neuroimaging	–	NA	NA	+	(1)Mild ventricular enlargement of prominent sulci suggestive of low brain volumes (2) Thinned corpus callosum (3) There is evidence of subependymal nodular heterotopia along the bilateral lateral ventricles anteriorly (4) Irregular border to the ventricular system, raising the possibility of PVL
White matter abnormalities	–	NA	NA	+ (subcortical T2-hyperintensities)	volume loss in the periventricular white matter
Other	–	NA	NA	Optic nerve head flattening	NA
Metabolic profile	high lactate and ammonia	NA	NA	NA	NA

F, female; FS, febrile seizures; M, male; NA, not available; RPE, retinal pigmented epithelium; y, years.

10.3389/fnmol.2024.1222935

TABLE 2 *SLITRK3* intragenic variants identified in our cohort.

	Patient ID	Probands F1-II:1, II:2, II:3	Proband F2-II:1	Proband F3-II:1
Variant annotation	GRCh38/hg38	3:165189015G > T	3:165189135T > C	3:165190146-165190171del
	position			
	(DNA change)			
	cDNA change (NM_001318810.2)	c.1816G > T	c.1696T > C	c.660_684del25
	Protein change	p.Glu606*	p.Cys566Arg	p.Gly221Trp*fs**15
	Inheritance, zygosity	AR, Hom	AD, Het	AD, Het
	dbSNP ID	–	–	–
	Region of Homozygosity (ROH)	37 Mb	N/A	N/A
	Variant seen in family	F1	F2	F3
Allele frequencies (PM2)	gnomAD v3	–	–	–
	(highest subpopulation)			
	gnomAD v2.1.1	–	–	–
	(highest subpopulation)			
	Frequency in ensembl browser	–	–	–
	GeneDX	–	1/145998	1/282424
	UK Brain bank	–	–	–
	Geno2MP	–	–	–
	Iranome	–	–	–
	GME Variome	–	–	–
	Frequency in in-house database‡	–	–	–
In silico predictions (PP3)	GERP	0.9	0.92	–
	CADD	36	28	–
	Polyphen-2	–	0.986 (PD)	–
	SIFT	–	0 (D)	–
	Provean	−8.729 (D)	−11.723 (D)	−4.851 (D)
	MutationTaster	1 (DC)	0.99 (DC)	1 (DC)
	Clinical significance	Pathogenic (PP1, PM2, PS3, PVS1)	Likely Pathogenic (PM2, PS2, PS3)	Likely Pathogenic (PM2, PS2)

TABLE 3 SLITRK3 KO mice exhibit postnatal lethality.

Genetic background	sex	*ST3 + / + (WT)*	*ST3 ± (HET)*	*ST3-/- (KO)*	total	χ 2-test: Mendelian	χ 2-test: B6N1-N2
B6N1-N2	Total	280 (28.8%)	527 (54.2%)	166 (17.1%)	973 (100%)	5.43E-08	
B6N8	Male	30 (31.9%)	54 (57.4%)	10 (10.6%)	94 (100%)	5.00E-03	2.49E-01
	Female	34 (42.5%)	39 (48.8%)	7 (8.8%)	80 (100%)	1.08E-04	1.16E-02
	Total	64 (36.8%)	93 (53.4%)	17 (9.8%)	174 (100%)	2.03E-06	9.51E-03

Genotype counts and percentages of progenies generated by inter-heterozygous mating. Genotyping was performed for B6N1/N2 progenies and B6N8 progenies at the ages of 4.1−7.0 weeks old.

in regulating GABAergic synapses, leading to a number of neurological consequences in human patients.

In keeping with its essential role in GABAergic synapse development, SLITRK3 is widely expressed in all brain regions from early development, with the highest levels found in the cerebral cortex and cerebellum (BRAINEAC database). The gene is intolerant to loss of function mutations in humans, with a pLi score of 0.94. Indeed, the mIPSC frequency and amplitude in hippocampal neurons expressing SLITRK3-E606X mutant had no changes compared with the control cells expressing WT SLITRK3 that increased inhibitory transmission. Consistently, expression of SLITRK3-E606X did not change dendritic densities of vGAT and gephyrin, while overexpression of WT SLITRK3 significantly increased GABAergic synapse development. These data indicate

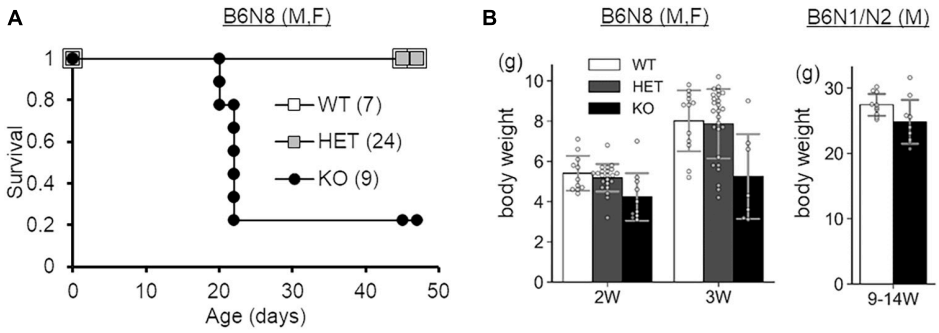

FIGURE 4
Survival and development of SLITRK3 KO mice. **(A)** Survival analysis. **(B)** Body weight at indicated ages. W, weeks-old. Open squares and bars, WT; gray squares and bars, heterozygote; closed squares and bars, KO. Error bars, SD. The numbers in parenthesis indicate n (the number of mice) in each group. Gray circles on bar graphs indicate the individual values of each mouse.

that E606X mutation abolishes the function of SLITRK3 in promoting GABAergic synapse development. We thus conclude that the phenotype in the index probands with the SLITRK3-E606X variant could be due to a loss of function of WT-SLITRK3. This could be explained by the fact that E606X is a truncation mutant lacking the important transmembrane domain and C-terminus.

Interestingly, the expression of the SLITRK3-C566R mutant also did not change mIPSCs and GABAergic density in hippocampal neurons, suggesting that the N-terminal residue, C566, may have an important role in the function of SLITRK3. The mutation of Cytosine 566 to Arginine is unable to promote inhibitory synaptic transmission as observed by the deficit in increasing GABAergic synaptic density (Figure 2). In line with SLITRK3 being tolerant to missense mutations in humans, with a Z-score of 0.59, we speculate that probably heterozygous *de novo* non-synonymous variants likely affect the protein function and have a potential role in disease. Currently, the mechanisms underlying the role of C566 in regulating inhibitory synapses remain unclear. As SLITRK3 N-terminus is critical for trans-synaptic interaction with presynaptic PTPδ and cis interaction with postsynaptic NL2, C566 might be important for SLITRK3 N-terminus mediated protein interactions crucial for its synaptogenic function.

Additionally, the overexpression studies showed no changes in dendritic densities of vGAT and gephyrin, suggesting these both variants SLITRK3-C566R and SLITRK3-E606X are essential to the function of SLITRK3 in the regulation of GABAergic synaptic densities. Together, we found the increased vGAT and gephyrin in neurons overexpressing SLITRK3-WT-Myc but no change of those in neurons overexpressing SLITRK3-C566R-Myc or SLITRK3-E606X-Myc, consistent with the change of mIPSC frequency in those transfected GFP-positive cultured hippocampal neurons.

Based on the HEK-293 cell ICC experiments investigating the co-localization ratio on the surface and the expression pattern with Golgi marker labeling, we observed that the E606 and C566 sites of the SLITRK3 protein are critical to the surface trafficking of the protein (Figure 3). Taken together with previous electrophysiology and immunostaining data in neurons (Figures 1, 2), these data further support the important role of human variants C566R and E606X in inhibitory synaptic transmissions.

In terms of seizure-associated phenotypes of SLITRK3 KO mice, we previously reported enhanced susceptibility to pentylenetetrazole-induced seizure and the appearance of spontaneous epileptiform EEG (Takahashi et al., 2012). These results together with the developmental deficits shown in the current study strongly support the *SLITRK3* loss-of-function mutations as genetic causes of epileptic encephalopathy. In addition, the cognitive dysfunction observed in SLITRK3 KO mice might pinpoint to the physiological function of the protein, as similar manifestations of sensory/motor signs or intellectual disability were present in the three siblings with the *SLITRK3* nonsense mutation.

Parvalbumin (PV) interneurons in the hippocampus are mostly basket cells with fast-spiking actions at a high energy cost, are highly vulnerable to stressors, and have been implicated in many neuropsychiatric disorders (Ruden et al., 2020). Impaired development or function of PV-positive interneurons is associated with epilepsy in various animal models of epilepsy, as well as some genetic forms of epilepsy in humans (Jiang et al., 2016). In mice, the selective silencing of hippocampal PV interneurons induces recurrent spontaneous limbic seizure (Drexel et al., 2017). Furthermore, reduced PV interneurons in SLITRK3 KO dentate gyrus could explain their hyperactivity and reduced anxiety-like behaviors because optogenetic activation of the dentate gyrus granule cells increases locomotive activity and open arm stayed time in elevated plus maze test (Kheirbek et al., 2013; Cho et al., 2022). Therefore, we speculate that deterioration of PV interneurons is associated with the neurological signs of the patients with SLITRK3 loss-of-function mutations.

The clinical phenotypes that are reported in this study and which are associated with the identified *SLITRK3* variants could be linked with the cellular deficits observed in our assays. Both c.1816G > T(p.Glu606*) and c.1696T > C (p.Cys566Arg) are unable to promote inhibitory synaptic transmission and have deficits in increasing GABAergic synaptic density (Figure 2). This correlated with absent protein levels and a shorter protein missing the cytoplasmic domain in the case of c.1816G > T(p.Glu606*) which is also reflected by impaired protein stability as suggested by *in silico* structural modeling (Figure 1E). However, in the case of c.1696T > C (p.Cys566Arg) and c.660_684del25(p.Gly221Trp*fs**15), this points more toward

10.3389/fnmol.2024.1222935

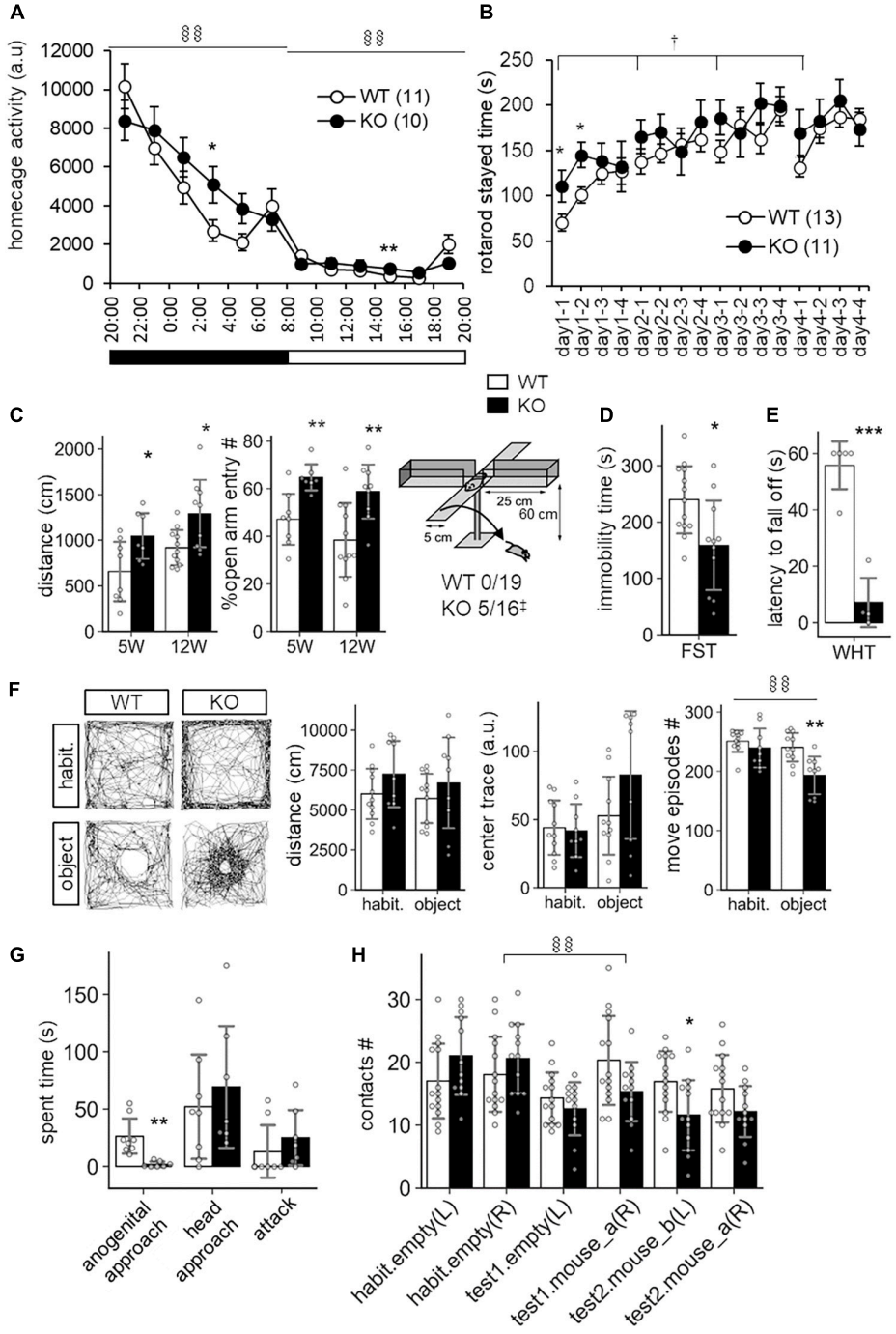

FIGURE 5

Behavioral abnormalities of SLITRK3 KO mice. **(A)** Spontaneous activities in homecages. $^{§§}P_{(genotype \times time)} < 0.01$; in two-way repeated-measures ANOVA (time and genotype as main factors). **(B)** Rotarod test. The tests are carried out daily from day 1 to day 4 (4 trials per day). The stayed time on accelerating rotarod is measured. $^{\dagger}P_{(genotype)} < 0.05$; in two-way repeated-measures ANOVA (1st trial and genotype as main factors). **(C)** Elevated plus maze test. (*Left*) Total distance traveled. (*Middle*) Percentages of the numbers of open arm entries to total arm entries. (*Right*) Falling off from open arms. Values indicate (number of fallen mice)/(total number of mice). ‡$p < 0.05$ in Fisher's exact test. **(D)** Immobility time in forced swim test (FST). Immobile time in the test was 10 min. **(E)** Wire hanging test (WHT). Latency to fall off from wire mesh after flipping was measured. **(F)** Novel object approach test. In the habituation session (*habit.*), mice were left in an open field for 15 min. In the novel object session (*object*), mice were left in an open field with an unfamiliar object (inverted paper cup) for 15 min. Traveled distance (*left*), trace (*middle*), and number of move episodes (*right*) during each session were measured. $^{§§}P_{(session \times time)} < 0.01$; in two-way repeated-measures ANOVA (session and genotype as main factors). **(G)** Resident intruder test. Times spent in approaching the anogenital region (*anogenital approach*) or head region (*head approach*) of intruder mice, and that in biting intruder mice (*attack*) were measured. **(H)** Social discrimination test. The graph indicates the number of contacts to cylinder cages with or without a mouse. The test consisted of three successive 15 min sessions: habituation session (*habit.*), two empty cages at the left and right corners; *test1* session, one empty cage on the left and a new mouse-containing cage at the right; *test2* session, a new mouse containing cage at left and a familiar mouse containing cage at right. $^{§§}P_{(session \times time)} < 0.01$; in two-way repeated-measures ANOVA (session and genotype as main factors). **(A–H)** *$p < 0.05$; **$p < 0.01$; ***$p < 0.001$ in unpaired two-tailed Student's *t*-test. Mean values are indicated in all graphs. *Open bars and circles*, WT; *closed bars and circles*, KO; *Error bars*, SD (bar graphs), SEM (line graphs). *Gray circles on bar graphs* indicate the individual value of each mouse. The *numbers in parentheses* in line graphs indicate *n* (the number of mice) in each experimental group.

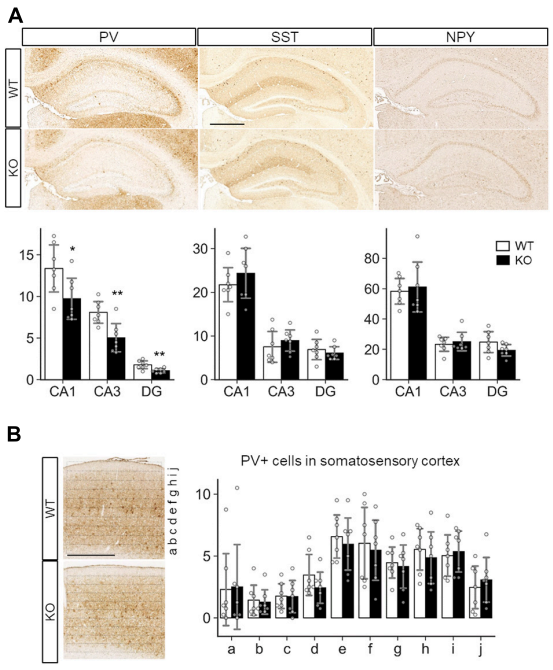

FIGURE 6
Quantitative analysis of inhibitory neuron subtypes in SLITRK3 KO brains. **(A)** Representative images for parvalbumin (PV), somatostatin (SST), and neuropeptide Y (NPY) immunostaining of the hippocampus CA1 stratum radiatum (CA1), CA3 stratum lucidum (CA3), dentate gyrus (DG) from P10-P16 WT (n = 7 mice) and KO (n = 7 mice) coronal sections. Sex-matched littermates WT and KO pairs (4 male pairs and 3 female pairs) were subjected to analysis. Quantitative analysis is outlined for each inhibitory neuron subgroup. **(B)** PV-positive cells in WT or KO somatosensory cortices were counted in ten strips (a-j) parallel to the pia surface. Immunopositive cells were counted by genotype-blinded observers. *Open bars*, WT; *closed bars*, KO; *Error bars*, SD. *Gray circles* indicate the individual values of each mouse, which are means of four independent images. *$p < 0.05$; **$p < 0.01$ in unpaired two-tailed Student's t-test.

altered structural confirmation of the proteins. Disulfide bonds can have profound effects on the folding pathway and the stability of a protein, thus increasing its suitability for existence in the extracellular milieu. However, due to the limited tendency of alpha-helical residues to form disulfide bridges in these two variants, we suspect that only a chunk of the extracellular domain is being formed, especially in the case of c.660_684del25, p.Gly221Trp*fs**15, which is predicted to be detrimental to normal protein function. Most Slitrk substitutions represent loss-of-function mutations that perturb the normal folding and/or glycosylation of Slitrks, In the case of c.1696T > C (p.Cys566Arg) which migrated slightly slower than the WT protein in the Western blot assay (Figure 2A), we do not have evidence for altered glycosylation causing aberrant protein trafficking, however, misfolding of the mutated protein could result in accumulation of defective SLITRK3 protein in the intracellular compartment of the Golgi apparatus (Figure 3).

In conclusion, this study identified a neurodevelopmental disease with an early onset of symptoms that is variably associated with additional neurological features predominated by GDD/ID, ADHD, hypotonia, and epilepsy. Given that the synaptopathies are defined as brain disorders associated with synaptic dysfunction (Grant, 2019) and that the individuals presented in this study have clinical features overlapping those observed in individuals with synaptopathies (cognitive disorders such as intellectual disability, motor dysfunction such as ataxia and dystonia, epilepsy and psychiatric diseases such as ASD and ADHD), we coin the phenotypes associated with *SLITRK3* variants as SLITRK3-related synaptopathy. Furthermore, variability in the effects of different *SLITRK3* mutants under *in vitro* conditions points toward mutation-specific mechanisms underlying the postsynaptic defect of the affected children, and this variability highlights a promising area of future research.

Data availability statement

The datasets presented in this study can be found in online repositories. The names of the repository/repositories and accession number(s) can be found below: https://databases.lovd.nl/shared/genes/SLITRK3.

Ethics statement

The studies involving humans were approved by the University College Hospital London (REC reference number: 07/Q0512/26, UCLH Project ID Number: 07/N018). The studies were conducted in accordance with the local legislation and institutional requirements. Written informed consent for participation in this study was provided by the participants' legal guardians/next of kin. The animal studies were approved by Animal Experiment Committees at the RIKEN Brain Science Institute and Animal Care and Use Committee of Nagasaki University. The studies were conducted in accordance with the local legislation and institutional requirements. Written informed consent was obtained from the owners for the participation of their animals in this study. Written informed consent was obtained from the minor(s)' legal guardian/next of kin for the publication of any potentially identifiable images or data included in this article.

Author contributions

SE: Conceptualization, Data curation, Formal analysis, Investigation, Visualization, Methodology, Writing—original draft, and Writing—review & editing. WH: Data curation, Formal analysis, Investigation, Visualization, and Methodology, Writing—review & editing. MI, MI, NV, CM, KM, CR, and TP: Data curation and Formal analysis. JL, NT, and HM: Data curation, Formal analysis, Investigation, Visualization and Methodology. YY, SL, EM, HL, GZ, FZ, NR, and PS: Data curation, Formal analysis, Investigation, and Methodology. MS: Methodology, Writing—original draft, and Writing—review & editing. NM: Methodology and Writing—review & editing. RM: Conceptualization and Methodology. VS: Data curation, Investigation, and Methodology. ML: Conceptualization. JA, WL, and HH: Conceptualization, Supervision, Funding acquisition, and Writing—review & editing. All authors contributed to the article and approved the submitted version.

Funding

The HH lab is supported by the MRC (MR/S01165X/1, MR/S005021/1, and G0601943), The National Institute for Health Research University College London Hospitals Biomedical Research Centre, Rosetree Trust, Ataxia UK, MSA Trust, Brain Research UK, Sparks GOSH Charity, Muscular Dystrophy UK (MDUK), Muscular Dystrophy Association (MDA USA). The JA lab is supported by the Japan Society for the Promotion of Science and MEXT (20K21605, 19H03327). WL lab is supported by NIH Intramural Research Program.

Acknowledgments

The original family data were collected as part of the SYNaPS Study Group collaboration funded by the Wellcome Trust and strategic award (Synaptopathies) funding (WT093205 MA and WT104033AIA). This research was conducted as part of the Queen Square Genomics group at University College London, supported by the National Institute for Health Research University College London Hospitals Biomedical Research Centre.

Conflict of interest

TP was an employee of GeneDx.

The remaining authors declare that the research was conducted in the absence of any commercial or financial relationships that could be construed as a potential conflict of interest.

Publisher's note

Supplementary material

The Supplementary Material for this article can be found online at: https://www.frontiersin.org/articles/10.3389/fnmol.2024.1222935/full#supplementary-material

References

Aruga, J., and Mikoshiba, K. (2003). Identification and characterization of Slitrk, a novel neuronal transmembrane protein family controlling neurite outgrowth. *Mol. Cell. Neurosci.* 24, 117–129. doi: 10.1016/s1044-7431(03)00129-5

Aruga, J., Yokota, N., and Mikoshiba, K. (2003). Human SLITRK family genes: Genomic organization and expression profiling in normal brain and brain tumor tissue. *Gene* 315, 87–94. doi: 10.1016/s0378-1119(03)00715-7

Bollig-Fischer, A., Bao, B., Manning, M., Dyson, G., Michelhaugh, S. K., Mittal, S., et al. (2021). Role of novel cancer gene SLITRK3 to activate NTRK3 in squamous cell lung cancer. *Mol. Biomed.* 2:26. doi: 10.1186/s43556-021-00051-2

Cherubini, E., Di Cristo, G., and Avoli, M. (2021). Dysregulation of GABAergic signaling in neurodevelomental disorders: Targeting cation-chloride co-transporters to re-establish a proper E/I balance. *Front. Cell. Neurosci.* 15:813441. doi: 10.3389/fncel.2021.813441

Cho, W. H., Noh, K., Lee, B. H., Barcelon, E., Jun, S. B., Park, H. Y., et al. (2022). Hippocampal astrocytes modulate anxiety-like behavior. *Nat. Commun.* 13:6536.

Clarkson, M. J., Zombori, G., Thompson, S., Totz, J., Song, Y., Espak, M., et al. (2015). The NifTK software platform for image-guided interventions: Platform overview and NiftyLink messaging. *Int. J. Comput. Assist. Radiol. Surg.* 10, 301–316. doi: 10.1007/s11548-014-1124-7

de Wit, J., and Ghosh, A. (2016). Specification of synaptic connectivity by cell surface interactions. *Nat. Rev. Neurosci.* 17, 22–35.

Drexel, M., Romanov, R. A., Wood, J., Weger, S., Heilbronn, R., Wulff, P., et al. (2017). Selective silencing of hippocampal parvalbumin interneurons induces development of recurrent spontaneous limbic seizures in mice. *The Journal of Neuroscience.* 37, 8166–8179. doi: 10.1523/JNEUROSCI.3456-16.2017

Efthymiou, S., Salpietro, V., Malintan, N., Poncelet, M., Kriouile, Y., Fortuna, S., et al. (2019). Biallelic mutations in neurofascin cause neurodevelopmental impairment and peripheral demyelination. *Brain* 142, 2948–2964. doi: 10.1093/brain/awz248

Gomez-Castro, F., Zappettini, S., Pressey, J. C., Silva, C. G., Russeau, M., Gervasi, N., et al. (2021). Convergence of adenosine and GABA signaling for synapse stabilization during development. *Science* 374:eabk2055. doi: 10.1126/science.abk2055

Grant, S. G. (2019). Synapse diversity and synaptome architecture in human genetic disorders. *Hum. Mol. Genet.* 28, R219–R225.

Gu, X., Mao, X., Lussier, M. P., Hutchison, M. A., Zhou, L., Hamra, F. K., et al. (2016). GSG1L suppresses AMPA receptor-mediated synaptic transmission and uniquely modulates AMPA receptor kinetics in hippocampal neurons. *Nat. Commun.* 7:10873. doi: 10.1038/ncomms10873

Han, W., Li, J., Pelkey, K. A., Pandey, S., Chen, X., Wang, Y. X., et al. (2019). Shisa7 is a GABAA receptor auxiliary subunit controlling benzodiazepine actions. *Science* 366, 246–250. doi: 10.1126/science.aax5719

Jiang, X., Lachance, M., and Rossignol, E. (2016). Involvement of cortical fast-spiking parvalbumin-positive basket cells in epilepsy. *Prog. Brain Res.* 226, 81–126. doi: 10.1016/bs.pbr.2016.04.012

Kang, H., Han, K. A., Won, S. Y., Kim, H. M., Lee, Y. H., Ko, J., et al. (2016). Slitrk missense mutations associated with neuropsychiatric disorders distinctively impair slitrk trafficking and synapse formation. *Front. Mol. Neurosci.* 9:104. doi: 10.3389/fnmol.2016.00104

Kheirbek, M. A., Drew, L. J., Burghardt, N. S., Costantini, D. O., Tannenholz, L., Ahmari, S. E., et al. (2013). Differential control of learning and anxiety along the dorsoventral axis of the dentate gyrus. *Neuron* 77, 955–968. doi: 10.1016/j.neuron.2012.12.038

Ko, J. (2012). The leucine-rich repeat superfamily of synaptic adhesion molecules: LRRTMs and Slitrks. *Mol. Cells* 34, 335–340. doi: 10.1007/s10059-012-0113-3

Ko, J., Choii, G., and Um, J. W. (2015). The balancing act of GABAergic synapse organizers. *Trends Mol. Med.* 21, 256–268.

Li, J., Han, W., Pelkey, K. A., Duan, J., Mao, X., Wang, Y. X., et al. (2017). Molecular dissection of neuroligin 2 and slitrk3 reveals an essential framework for GABAergic synapse development. *Neuron* 96, 808–826.e8. doi: 10.1016/j.neuron.2017.10.003

Li, J., Han, W., Wu, K., Li, Y. D., Liu, Q., and Lu, W. (2019). A conserved tyrosine residue in slitrk3 carboxyl-terminus is critical for GABAergic synapse development. *Front. Mol. Neurosci.* 12:213. doi: 10.3389/fnmol.2019.00213

Linde, J., and Zimmer-Bensch, G. (2020). DNA methylation-dependent dysregulation of GABAergic interneuron functionality in neuropsychiatric diseases. *Front. Neurosci.* 14:586133. doi: 10.3389/fnins.2020.586133

Meziane, H., Ouagazzal, A. M., Aubert, L., Wietrzych, M., and Krezel, W. (2007). Estrous cycle effects on behavior of C57BL/6J and BALB/cByJ female mice: Implications for phenotyping strategies. *Genes Brain Behav.* 6, 192–200. doi: 10.1111/j.1601-183X.2006.00249.x

Nyul, L. G., Udupa, J. K., and Zhang, X. (2000). New variants of a method of MRI scale standardization. *IEEE Trans. Med. Imaging* 19, 143–150.

Powell, N. M., Modat, M., Cardoso, M. J., Ma, D., Holmes, H. E., Yu, Y., et al. (2016). Fully-automated muMRI morphometric phenotyping of the Tc1 mouse model of down syndrome. *PLoS One* 11:e0162974. doi: 10.1371/journal.pone.0162974

Proenca, C. C., Gao, K. P., Shmelkov, S. V., Rafii, S., and Lee, F. S. (2011). Slitrks as emerging candidate genes involved in neuropsychiatric disorders. *Trends Neurosci.* 34, 143–153. doi: 10.1016/j.tins.2011.01.001

Quinodoz, M., Peter, V. G., Bedoni, N., Royer Bertrand, B., Cisarova, K., Salmaninejad, A., et al. (2021). AutoMap is a high performance homozygosity mapping tool using next-generation sequencing data. *Nat. Commun.* 12:518. doi: 10.1038/s41467-020-20584-4

Ramamoorthi, K., and Lin, Y. (2011). The contribution of GABAergic dysfunction to neurodevelopmental disorders. *Trends Mol. Med.* 17, 452–462.

Raudvere, U., Kolberg, L., Kuzmin, I., Arak, T., Adler, P., Peterson, H., et al. (2019). g:Profiler: A web server for functional enrichment analysis and conversions of gene lists (2019 update). *Nucleic Acids Res.* 47, W191–W198. doi: 10.1093/nar/gkz369

Richards, S., Aziz, N., Bale, S., Bick, D., Das, S., Gastier-Foster, J., et al. (2015). Standards and guidelines for the interpretation of sequence variants: A joint consensus recommendation of the American College of Medical Genetics and Genomics and the Association for Molecular Pathology. *Genet. Med.* 17, 405–424.

Ruden, J. B., Dugan, L. L., and Konradi, C. (2020). Parvalbumin interneuron vulnerability and brain disorders. *Neuropsychopharmacology* 46, 279–287.

Shannon, P., Markiel, A., Ozier, O., Baliga, N. S., Wang, J. T., Ramage, D., et al. (2003). Cytoscape: A software environment for integrated models of biomolecular interaction networks. *Genome Res.* 13, 2498–2504. doi: 10.1101/gr.1239303

Sobreira, N., Schiettecatte, F., Valle, D., and Hamosh, A. (2015). GeneMatcher: A matching tool for connecting investigators with an interest in the same gene. *Hum. Mutat.* 36, 928–930. doi: 10.1002/humu.22844

Takahashi, H., Katayama, K., Sohya, K., Miyamoto, H., Prasad, T., Matsumoto, Y., et al. (2012). Selective control of inhibitory synapse development by Slitrk3-PTPdelta trans-synaptic interaction. *Nat. Neurosci.* 15, 389–398, S1–S2. doi: 10.1038/nn.3040

Tomkins, J. E., Ferrari, R., Vavouraki, N., Hardy, J., Lovering, R. C., Lewis, P. A., et al. (2020). PINOT: An intuitive resource for integrating protein-protein interactions. *Cell Commun. Signal.* 18:92. doi: 10.1186/s12964-020-00554-5

Turnbull, C., Scott, R. H., Thomas, E., Jones, L., Murugaesu, N., Pretty, F., et al. (2018). The 100 000 Genomes Project: Bringing whole genome sequencing to the NHS. *BMJ* 361:k1687.

Tustison, N. J., Avants, B. B., Cook, P. A., Zheng, Y., Egan, A., Yushkevich, P. A., et al. (2010). N4ITK: Improved N3 bias correction. *IEEE Trans. Med. Imaging* 29, 1310–1320.

Vavouraki, N., Tomkins, J., Kara, E., Houlden, H., Hardy, J., Tindall, M., et al. (2021). Integrating protein networks and machine learning for disease stratification in the Hereditary Spastic Paraplegias. *iScience* 24:102484. doi: 10.1016/j.isci.2021.102484

Wang, C. J., Zhang, Z. Z., Xu, J., Wang, M., Zhao, W. Y., Tu, L., et al. (2015). SLITRK3 expression correlation to gastrointestinal stromal tumor risk rating and prognosis. *World J. Gastroenterol.* 21, 8398–8407. doi: 10.3748/wjg.v21.i27.8398

Won, S. Y., Lee, P., and Kim, H. M. (2019). Synaptic organizer: Slitrks and type IIa receptor protein tyrosine phosphatases. *Curr. Opin. Struct. Biol.* 54, 95–103.

Yang, J., Yan, R., Roy, A., Xu, D., Poisson, J., and Zhang, Y. (2015). The I-TASSER Suite: Protein structure and function prediction. *Nat. Methods* 12, 7–8. doi: 10.1038/nmeth.3213

Yim, Y. S., Kwon, Y., Nam, J., Yoon, H. I., Lee, K., Kim, D. G., et al. (2013). Slitrks control excitatory and inhibitory synapse formation with LAR receptor protein tyrosine phosphatases. *Proc. Natl. Acad. Sci. U.S.A.* 110, 4057–4062.